Supporting Information for

Separation of *o*-vanillin hydrazone isomers constructing Dy_2 single-molecule magnet and Dy_3 single-molecule toroic

Linghao Meng,[a,b] Xu Ying,[c] Jinjiang Wu,[d]* Zhenhua Zhu,[b] Xiao-Lei Li,[b] Yunquan Wang,[a,b] Peng Zhang[a,b]* and Jinkui Tang[a,b,c]*

[a] School of Applied Chemistry and Engineering, University of Science and Technology of China, Hefei 230026, P. R. China.
[b] State Key Laboratory of Rare Earth Resource Utilization, Changchun Institute of Applied Chemistry, Chinese Academy of Sciences, Changchun 130022, P. R. China.
[c] School of Chemistry and Chemical Engineering, Beijing Institute of Technology, Beijing 102488, P. R. China.
[d] School of Chemistry and Chemical Engineering, North University of China, Taiyuan 030051, P. R. China.
*E-mail: jtang@bit.edu.cn, pengzhang@ciac.ac.cn, sa175010@mail.ustc.edu.cn

Contents

1. Synthesis and characterization

General procedure

Unless otherwise noted, all oxygen or moisture sensitive reactions were conducted in dried glassware under an atmosphere of nitrogen or argon. All the solvents and reagents purchased from commercial sources were used without further purification. All coordination reaction manipulations described were carried out under ambient atmosphere. *O*-vanilloyl hydrazine (**S1**) and Ethyl 2-oxo-2-(pyridin-2-yl)acetate (**S2**) were synthesized according to the published method.[1, 2] Thin-layer Chromatography (TLC) was performed on aluminum sheets precoated with 0.25 mm thick silica gel GF254 (Shanghai Shengya Chemicals (China)) and visualized by exposure to ultraviolet light. Chromatographic purification of products was accomplished using forced-flow chromatography on 200-300 mesh silica gel.

Measurements

^{1}H NMR spectra and ^{13}C NMR spectra were recorded on Bruker Avance 400 MHz spectrometer. Chemical shifts are reported in parts per million relative to the residual proton signal of the solvent CD_3OD (3.31 ppm) and DMSO-d_6 (2.50 ppm). Elemental analyses (C, H, N, S) were performed on a Perkin-Elmer 2400 analyzer. FT-IR spectra were recorded with a Nicolet 6700 Flex FTIR spectrometer equipped with a smart iTR attenuated total reflectance (ATR) sampling accessory in the range from 4000 to 535 cm^{-1}. UV-Vis spectra were performed on UV-1750 UV-Vis spectrophotometer. Light irradiation was performed in the NMR tube using a CSD-D64KXY lamp (P = 2.2 W) for 5 hours. The sample was placed at a distance of 5 cm from the light source. The magnetic data for the **Dy_3** and **Dy_2** complexes were measured using a Quantum Design MPMS-XL7 SQUID magnetometer and a Quantum Design MPMS3 magnetometer, respectively. For **Dy_3** complex, Direct current (DC) magnetic susceptibility and magnetization data were recorded on a Quantum Design MPMS-XL7 SQUID magnetometer equipped with a 7 T magnet. Variable-temperature magnetic susceptibility ware collected with an external magnetic field of 1000 Oe in the temperature range of 2-300 K. Magnetic hysteresis loops were collected using a Quantum Design MPMS-XL7 SQUID magnetometer in 1.9 K. Alternating current (AC) magnetic susceptibility measurements were performed using a Quantum Design MPMS-XL7 SQUID magnetometer using an oscillating field of 3 Oe. For **Dy_2** complex, Direct current (DC) magnetic susceptibility and magnetization data were recorded on a Quantum Design MPMS3 SQUID magnetometer equipped with a 7 T magnet. Variable-temperature magnetic susceptibility ware collected with an external magnetic field of 1000 Oe in the temperature range of 2-300 K. Magnetic hysteresis loops were collected using a Quantum Design MPMS3 magnetometer in 1.9 K. Alternating current (AC) magnetic susceptibility measurements were performed using a Quantum Design MPMS3 magnetometer using an oscillating field of 2 Oe. The experimental magnetic susceptibility data were corrected for the diamagnetism estimated from Pascal's tables and sample holder calibration.[3]

Synthesis

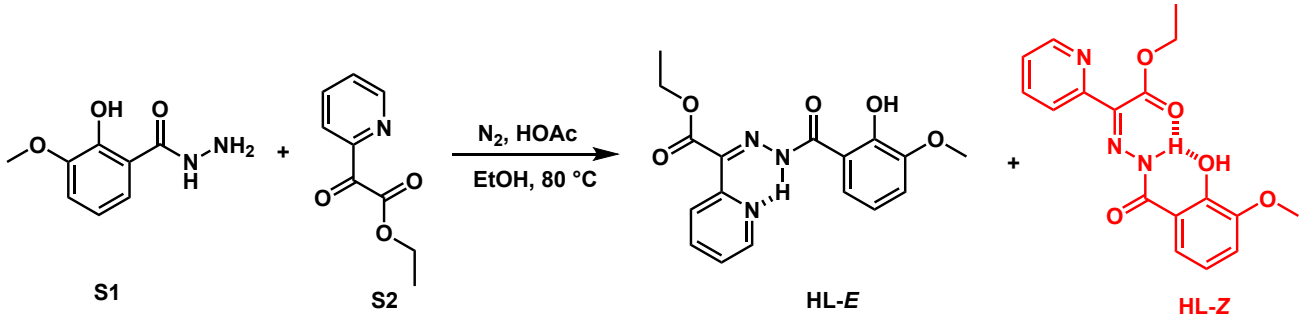

Scheme S1. Synthetic routes of HL-*E* and HL-*Z*.

Synthetic procedure for HL-*E* and HL-*Z*.

In a reaction flask, 50 mL of EtOH was added and bubbled for 15 min. Under a N_2 atmosphere, 1.82 g (10 mmol) of *o*-vanillin hydrazide (**S1**) and 2.0 g (13 mmol) of ethyl picolinoylacetate (**S2**) were added to the flask. After three cycles of evacuation and refilling with N_2, the mixture was heated to 80 °C until complete dissolution. Under a N_2 atmosphere, 200 μL(3.5 mmol) of acetic acid was added to the mixture. And then, the reaction was carried out at 80 °C for 12 h. After completion, the solution was cooled to room temperature, and the solvent was removed under reduced pressure. The resulting solid was dissolved in DCM and washed with $NaHCO_3$ solution until no acetic acid remained, followed by washing with H_2O and saturated NaCl solution. The organic phase was dried over anhydrous Na_2SO_4, filtered off the anhydrous Na_2SO_4 and concentrated under reduced pressure. The crude product was purified by column chromatography over silica gel (200–300 mesh) using a mixture of petroleum ether, DCM, and ethyl acetate (10:10:1, v/v/v) as eluent, yielding yellow granular product HL-*E* and green powdered product HL-*Z* with yields of 1.75 g (35%) and 1.5 g (30%), respectively. HL-*E*. **^{1}H NMR** (400 MHz, DMSO-*d*6) δ (ppm): 15.05 (s, 1H, N-H), 10.73 (s, 1H, H2), 9.03 (d, J = 4.4 Hz, 1H, H10), 8.07 (td, J = 8.0, 2.0 Hz, 1H, H8), 7.75 (d, J = 8.0 Hz, 1H, H7), 7.64 – 7.58 (m, 1H, H9), 7.55 (d, J = 8.0 Hz, H6), 7.22 (dd, J = 8.0, 1.6 Hz, 1H, H4), 6.94 (t, J = 8.0 Hz, 1H, H5), 4.37 (q, J = 7.1 Hz, 2H, H11), 3.89 (s, 3H, H3), 1.34 (t, J = 7.1 Hz, 3H, H12). **^{13}C NMR** (101 MHz, DMSO-*d*6) δ (ppm): 164.52 (C15), 163.02 (C8), 149.01 (C10/C14), 148.17 (C2), 146.59 (C1), 138.38 (C9), 137.86 (C12), 124.76 – 115.56 (C3, C4, C5, C6, C11, C13), 61.64 (C16), 56.27 (C7), 14.01 (C17). HL-*Z*. **^{1}H NMR** (400 MHz, DMSO-*d*6) δ (ppm): 12.32 (s, 1H, N-H), 11.04 (s, 1H, H2), 8.60 (s, 1H, H10), 7.94 (m, 2H, H7/H8), 7.63 – 7.52 (d, J = 9.1 Hz, 1H, H6), 7.50 – 7.44 (dd, J = 8.8, 4.8 Hz, 1H, H9), 7.22 (d, J = 7.9 Hz, 1H, H4), 6.96 (t, J = 8.0 Hz, 1H, H5), 4.46 (q, J = 7.1 Hz, 2H, H11), 3.88 (s, 3H, H3), 1.31 (t, J = 7.1 Hz, 3H, H12). **^{13}C NMR** (101 MHz, DMSO-*d*6) δ (ppm):163.30 (C15), 162.73 (C8), 152.62 (C10), 149.57 (C2), 148.78 (C1), 146.64 (C14), 144.67 (C9), 137.74 (C12), 125.15 – 116.17 (C3, C4, C5, C6, C11, C13), 62.66 (C16), 56.74 (C7), 14.40 (C17).

Synthetic procedure for **Dy_3**

A mixture of HL-*E* (0.019 g, 0.05 mmol), $Dy(SCN)_3 \cdot 6H_2O$ (0.021 g, 0.05 mmol), and Et_3N (10.5 μL, 0.075 mmol) was dissolved in a mixed solvent of EtOH/DCM (8 mL/2 mL). After stirring for 2 h, the mixture was filtered, and the filtrate was collected. Slow diffusion of the filtrate at room temperature over one day yielded yellow transparent block crystals of **Dy_3** (0.013 g, 19.9% based on Dy). Elemental analysis (%) calculated for $C_{60}H_{65}Dy_3N_{13}O_{20.5}S_4$ (M_W = 1911.99): C, 37.98; H, 3.43; N, 9.52. S, 6.71. Found: C, 36.98; H, 3.21; N, 10.19, S, 7.05. FTIR ν/cm^{-1} (ATR): 2980 (vs), 2048 (m), 1715 (vs), 1619

(m), 1554 (m), 1500 (m), 1435 (m), 1368 (vs), 1314 (m), 1280 (m), 1216 (w), 1176 (m), 1101 (w), 1063 (m), 1003 (m), 937 (vs), 852 (m), 797 (m), 735 (w), 621 (m).

Synthetic procedure for **Dy_2**

A mixture of HL-*Z* (0.019 g, 0.05 mmol), $Dy(SCN)_3 \cdot 6H_2O$ (0.021 g, 0.05 mmol), and 1 M aqueous $NaHCO_3$ solution (75 μL, 0.075 mmol) was dissolved in a mixed solvent of EtOH/DCM (6 mL/3 mL). After stirring for 2 h, the mixture was filtered, and the filtrate was collected. Slow diffusion of the filtrate at room temperature over two weeks yielded red transparent block crystals of **Dy_2** (0.017 g, 17.4% based on Dy). Elemental analysis (%) calculated for $C_{70}H_{64}Dy_2N_{14}O_{20}S_2$ (M_W = 1954.6): C, 42.97; H, 3.27; N, 10.03, S, 3.27. Found: C, 42.26; H, 3.51; N, 10.03, S, 3.97. FTIR ν/cm^{-1} (ATR): 3662 (vs), 2987 (m), 2359 (vs), 2045 (m), 1727 (m), 1615 (m), 1594 (m), 1561 (vs), 1521 (m), 1442 (m), 1364 (m), 1325 (m), 1228 (w), 1191 (m), 1066 (w), 967 (m), 850 (m), 797 (m), 742 (m), 590 (m).

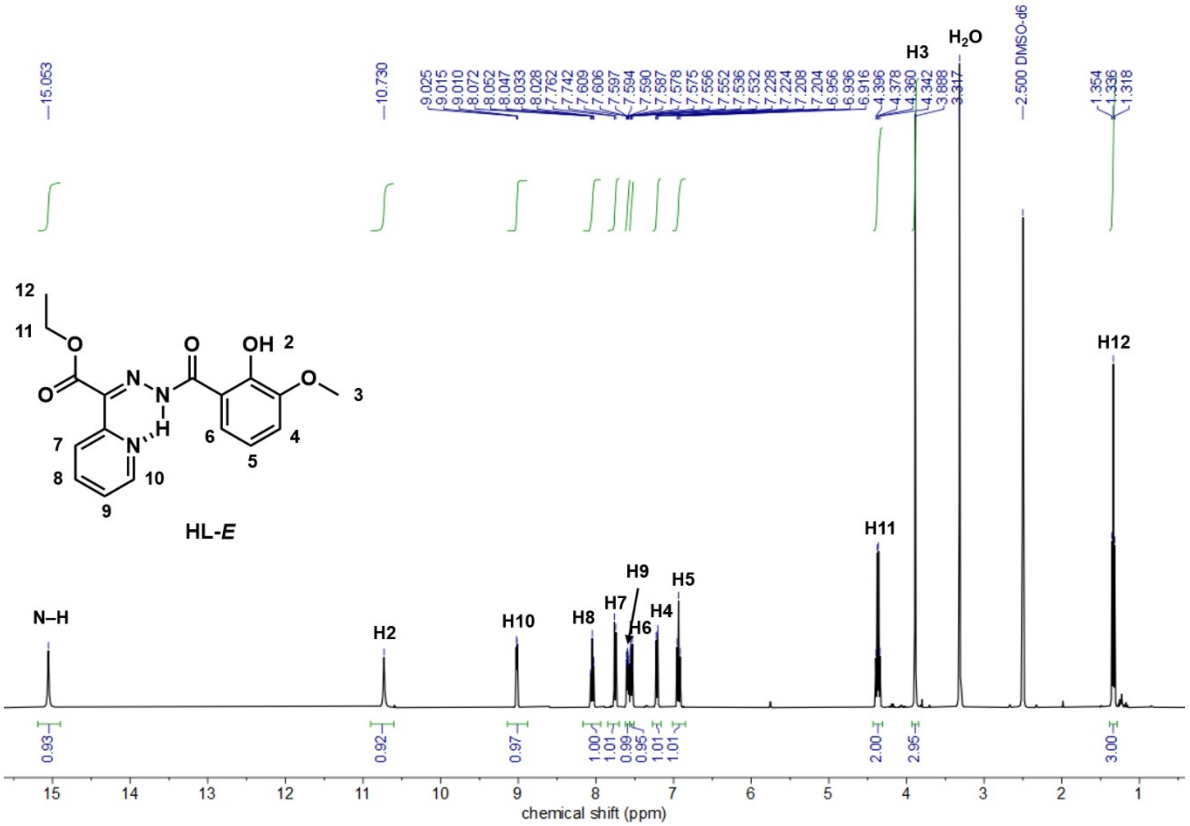

Figure S1. [1]H-NMR (400 MHz) spectrum of HL-*E* in DMSO-*d*6.

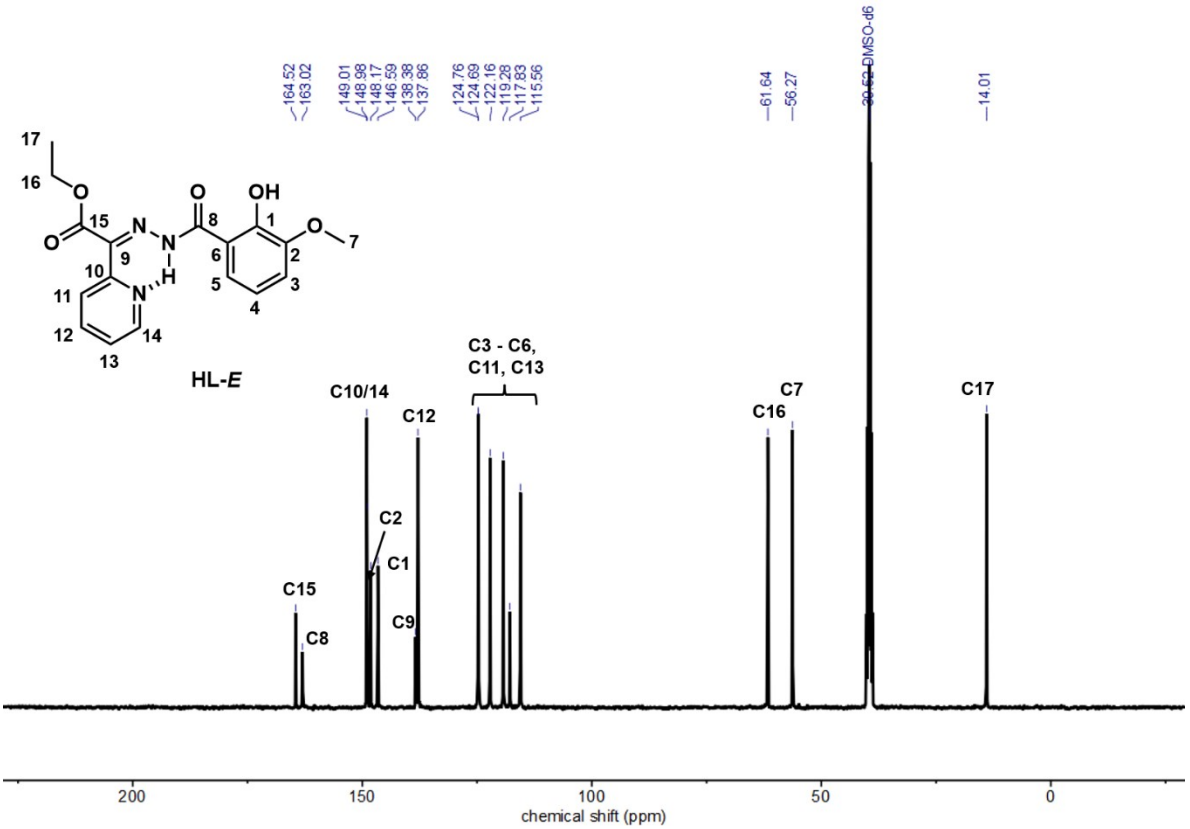

Figure S2. [13]C-NMR spectrum of HL-*E* in DMSO-*d*6.

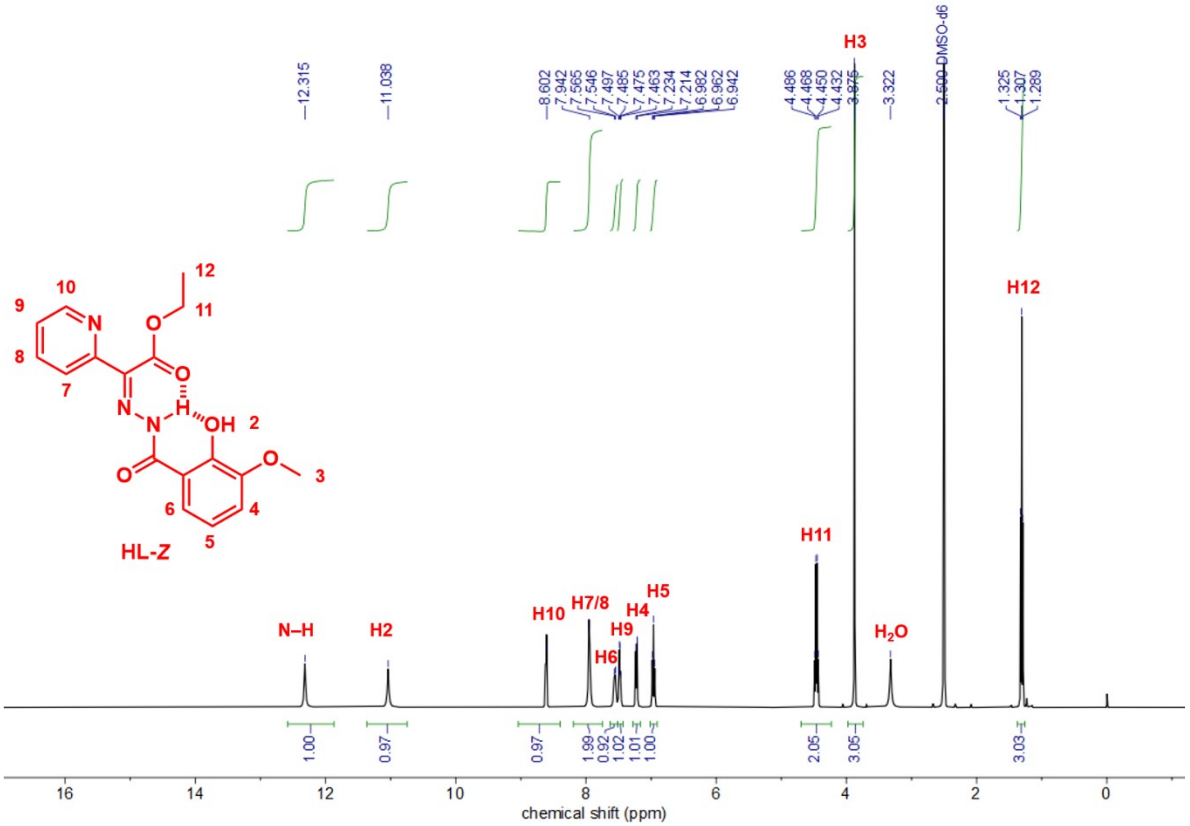

Figure S3. ^{1}H-NMR (400 MHz) spectrum of HL-*Z* in DMSO-*d*6.

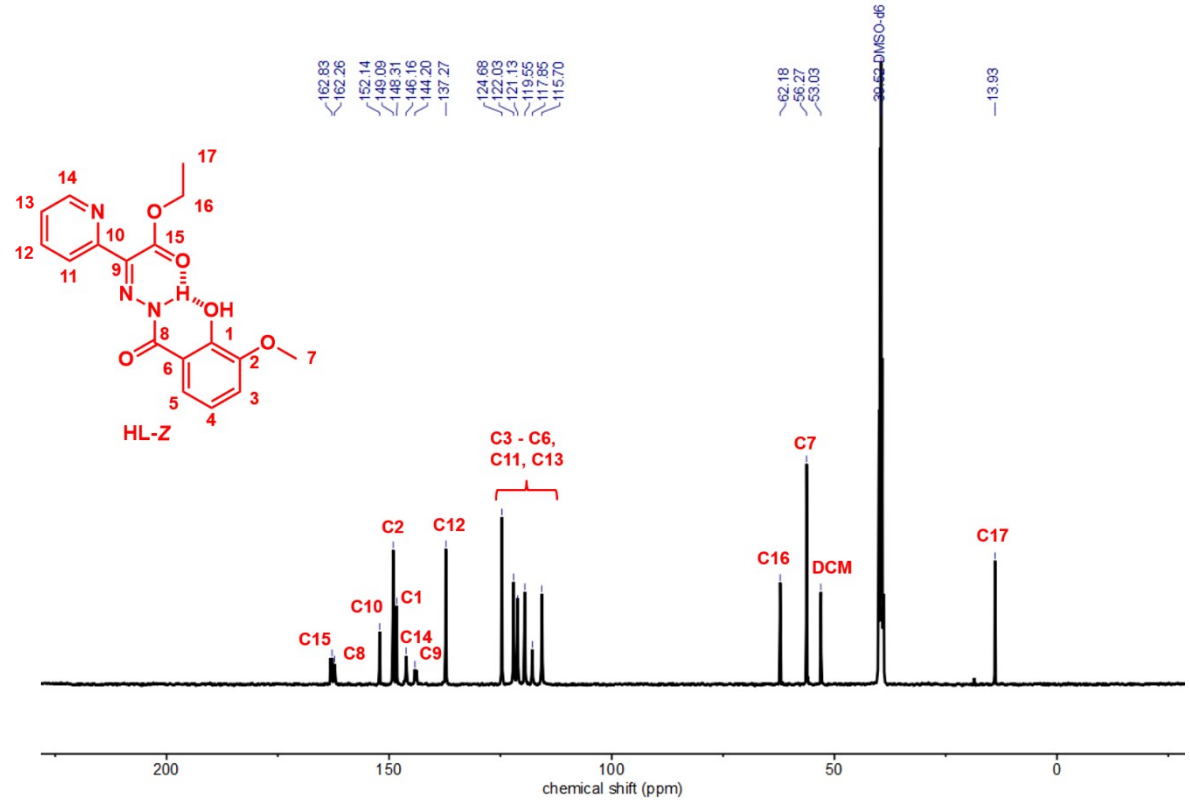

Figure S4. ^{13}C-NMR spectrum of HL-*Z* in DMSO-*d*6.

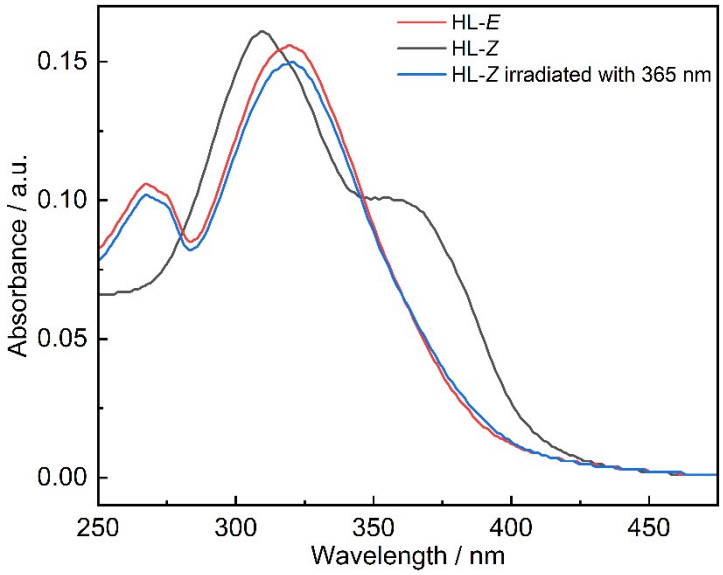

Figure S5. UV-vis spectra of HL-*E* (red), HL-*Z* (black) and HL-*Z* irradiated with 365 nm (blue) in MeOH ($c = 1.0 \times 10^{-5}$ M).

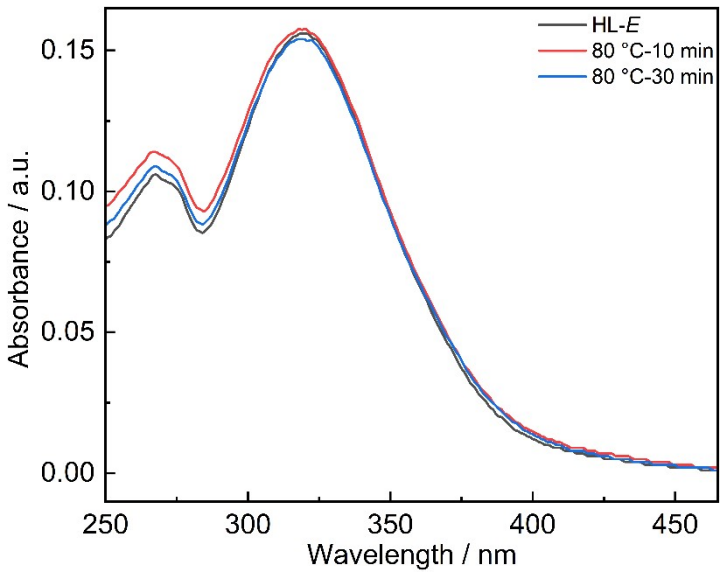

Figure S6. UV-vis spectra of HL-*E* (black) and HL-*E* after heating for 10 min (red) and 30 min (blue) in MeOH ($c = 1.0 \times 10^{-5}$ M).

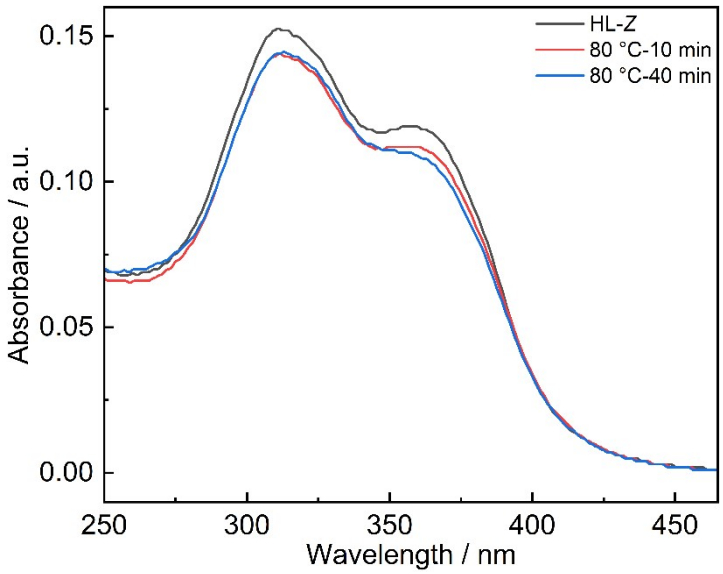

Figure S7. UV-vis spectra of HL-*Z* (black) and HL-*Z* after heating for 10 min (red) and 30 min (blue) in MeOH ($c = 1.0 \times 10^{-5}$ M).

2. X-ray crystallographic data

Single-crystal X-ray data for ligands HL-*E*, HL-*Z* and complexes **Dy_3**, **Dy_2** were recorded on a Bruker SMART APEX diffractometer equipped with graphite-monochromatized Cu Kα radiation (λ = 1.54178 Å) and Mo Kα radiation (λ = 0.71073 Å) at 180 K. The structures were solved in Olex2 with SHELXT using intrinsic phasing and were refined with SHELXL using least squares minimization.[4-6] All non-hydrogen atoms were refined anisotropically. All hydrogen atom positions were calculated geometrically and refined using the riding model. Crystallographic data, refinement details are given in Tables S1-S8.

Table S1. Crystal data and structure refinement for HL-*E* and HL-*Z*.

Compound reference	HL-*E*	HL-*Z*
Chemical formula	$C_{17}H_{17}N_3O_5$	$C_{17}H_{17}N_3O_5$
Formula Mass	343.33	343.33
Crystal system	orthorhombic	monoclinic
a (Å)	13.6818 (3)	14.3621 (6)
b (Å)	8.4637 (2)	13.3023 (7)
c (Å)	13.9314 (3)	16.4968 (7)
α (°)	90	90
β (°)	90	97.461 (2)
γ (°)	90	90
Unit cell volume (Å^3)	3926.2 (5)	3125.0 (2)
Temperature (K)	180.0	180.0
Space group	*P*ca2$_1$	*C*2/c
Z	4	8
ρ_{calc} (g/cm^3)	1.414	1.455
F (000)	720.0	1432.0
Radiation	CuKα (λ = 1.54178)	CuKα (λ = 1.54178)
Reflections collected	7347	14395
Independent reflections	2682	2731
R_{int}	0.0311	0.0527
GOF on F^2	1.070	1.397
R_1 (I ≥2 σ (*I*))	0.0315	0.1007
wR_2 (all data)	0.0816	0.3430
CCDC number	2516757	2516758

Table S2. Crystal data and structure refinement for **Dy_3** and **Dy_2**.

Compound reference	**Dy_3**	**Dy_2**
Chemical formula	$C_{60}H_{65}Dy_3N_{13}O_{20.5}S_4$	$C_{70}H_{64}Dy_2N_{14}O_{20}S_2$
Formula Mass	1911.99	1954.6
Crystal system	triclinic	monoclinic
a (Å)	14.9013 (9)	26.0695 (14)
b (Å)	16.1060 (11)	16.9341 (10)
c (Å)	18.0875 (13)	22.7465 (12)
α (°)	97.214 (3)	90
β (°)	100.611 (2)	124.476 (2)
γ (°)	109.959 (2)	90
Unit cell volume (Å^3)	3926.2 (5)	8278.0 (8)
Temperature (K)	180.0	180.0
Space group	*P*-1	*C*2/c
Z	2	4
ρ_{calc} (g/cm^3)	1.656	1.453
F (000)	1936.0	3624.0
Radiation	MoKα (λ = 0.71073)	MoKα (λ = 0.71073)
Reflections collected	79556	54965
Independent reflections	13901	8160
R_{int}	0.0483	0.0766
GOF on F^2	1.041	1.055
R_1 (I ≥2 σ (*I*))	0.0296	0.0614
wR_2 (all data)	0.752	0.2106
CCDC number	2516608	2516607

Table S3. Selected bond distances (Å) for **Dy_3**.

Dy_3			
Dy1-O1	2.3479(2)	Dy2-O7	2.282(3)
Dy1-O2	2.3750(2)	Dy2-O8	2.483(3)
Dy1-O3	2.334(3)	Dy2-O12	2.397(3)
Dy1-O5	2.326(3)	Dy2-N4	2.399(4)
Dy1-O6	2.466(3)	Dy3-O1	2.3785(2)
Dy1-O11	2.307(3)	Dy3-O2	2.3623(2)
Dy1-O13	2.394(3)	Dy3-O4	2.335(3)
Dy1-N3	2.385(4)	Dy3-O5	2.340(3)
Dy2-O1	2.3642(2)	Dy3-O9	2.289(3)
Dy2-O2	2.3546(2)	Dy3-O10	2.469(3)
Dy2-O3	2.321(3)	Dy3-N1	2.416(4)
Dy2-O4	2.337(3)	Dy3-N2	2.398(4)

Table S4. Selected bond distances (Å) for **Dy_2**.

Dy_2			
Dy1-O1	2.310(3)	Dy1-N2	2.471(3)
Dy1-O2	2.262(3)	Dy1-N3	2.536(3)
Dy1-O5	2.397(3)	Dy1-N6	2.571(3)
Dy1-N1	2.368(5)	Dy1-N7	2.596(4)

Table S5. Selected bond angles (°) for **Dy_3**.

Dy_3					
O1-Dy1-O2	60.907(5)	O1-Dy2-O8	130.41(7)	O1-Dy3-O10	129.66(8)
O1-Dy1-O6	125.75(7)	O1-Dy2-O12	78.16(8)	O1-Dy3-N1	75.68(9)
O1-Dy1-O13	134.42(8)	O1-Dy2-N4	137.00(9)	O1-Dy3-N2	137.73(10)
O1-Dy1-N3	79.07(10)	O2-Dy2-O1	60.968(6)	O2-Dy3-O1	60.655(5)
O2-Dy1-O6	129.36(7)	O2-Dy2-O8	124.74(7)	O2-Dy3-O10	125.82(7)
O2-Dy1-O13	73.86(8)	O2-Dy2-O12	138.64(8)	O2-Dy3-N1	136.07(9)
O2-Dy1-N3	139.31(10)	O2-Dy2-N4	76.27(9)	O2-Dy3-N2	77.16(10)
O3-Dy1-O1	72.55(7)	O3-Dy2-O1	72.48(7)	O4-Dy3-O1	72.77(7)
O3-Dy1-O2	73.96(7)	O3-Dy2-O2	74.57(7)	O4-Dy3-O2	74.24(7)
O3-Dy1-O6	64.54(9)	O3-Dy2-O4	141.62(10)	O4-Dy3-O5	141.41(9)
O3-Dy1-O13	90.74(11)	O3-Dy2-O8	154.01(9)	O4-Dy3-O10	153.96(10)
O3-Dy1-N3	102.16(13)	O3-Dy2-O12	100.17(11)	O4-Dy3-N1	98.40(12)
O5-Dy1-O1	74.66(7)	O3-Dy2-N4	93.01(12)	O4-Dy3-N2	94.47(13)
O5-Dy1-O2	72.86(7)	O4-Dy2-O1	73.01(7)	O5-Dy3-O1	73.84(7)
O5-Dy1-O3	141.55(10)	O4-Dy2-O2	74.36(7)	O5-Dy3-O2	72.85(7)
O5-Dy1-O6	153.89(10)	O4-Dy2-O8	64.37(9)	O5-Dy3-O10	64.59(10)
O5-Dy1-O13	98.18(12)	O4-Dy2-O12	88.68(10)	O5-Dy3-N1	91.56(13)
O5-Dy1-N3	90.71(13)	O4-Dy2-N4	100.93(12)	O5-Dy3-N2	97.34(13)
O11-Dy1-O1	137.94(8)	O7-Dy2-O1	128.97(8)	O9-Dy3-O1	130.32(8)
O11-Dy1-O2	129.56(8)	O7-Dy2-O2	137.25(7)	O9-Dy3-O2	136.06(8)
O11-Dy1-O3	145.74(10)	O7-Dy2-O3	71.79(10)	O9-Dy3-O4	71.72(10)
O11-Dy1-O5	72.40(10)	O7-Dy2-O4	145.63(10)	O9-Dy3-O5	146.71(10)
O11-Dy1-O6	81.77(10)	O7-Dy2-O8	82.71(10)	O9-Dy3-O10	82.47(10)
O11-Dy1-O13	76.17(12)	O7-Dy2-O12	73.67(11)	O9-Dy3-N1	76.40(13)
O11-Dy1-N3	75.94(14)	O7-Dy23-N4	79.91(12)	O9-Dy3-N2	78.65(13)
O13-Dy1-O6	78.82(12)	O12-Dy2-O8	76.76(11)	N1-Dy3-O10	78.28(12)
N3-Dy1-O6	79.18(13)	O12-Dy2-N4	144.84(12)	N2-Dy3-O10	76.72(13)
N3-Dy1-O13	146.50(13)	N4-Dy2-O8	77.25(12)	N2-Dy3-N1	146.58(14)

Table S6. Selected bond angles (°) for **Dy_2**.

Dy_2					
O1-Dy1-O5	84.29(10)	O2-Dy1-N3	77.13(10)	N1-Dy1-N6	144.09(13)
O1-Dy1-N1	87.63(13)	O2-Dy1-N6	70.81(10)	N1-Dy1-N7	82.66(13)
O1-Dy1-N2	64.77(11)	O2-Dy1-N7	92.08(11)	N2-Dy1-N3	63.60(10)
O1-Dy1-N3	128.16(11)	O5-Dy1-N2	68.24(10)	N2-Dy1-N6	119.01(11)
O1-Dy1-N6	76.47(10)	O5-Dy1-N3	81.23(11)	N2-Dy1-N7	135.62(12)
O1-Dy1-N7	73.74(12)	O5-Dy1-N6	62.51(10)	N3-Dy1-N6	134.86(12)
O2-Dy1-O1	147.24(11)	O5-Dy1-N7	123.67(11)	N3-Dy1-N7	150.97(12)
O2-Dy1-O5	79.35(10)	N1-Dy1-O5	148.39(12)	N6-Dy1-N7	62.14(12)
O2-Dy1-N1	120.35(13)	N1-Dy1-N2	80.67(13)		
O2-Dy1-N2	131.65(10)	N1-Dy1-N3	79.96(14)		

Table S7. The CShM values calculated by SHAPE 2.1 for **Dy_3**.[7, 8]

Central atom	Coordination Geometry	**Dy1**	**Dy2**	**Dy3**
Dy	Octagon (D_{8h})	30.931	31.949	31.122
	Heptagonal pyramid (C_{7v})	21.997	22.251	21.482
	Hexagonal bipyramid (D_{6h})	16.140	16.382	16.442
	Cube (O_h)	10.309	10.128	10.022
	Square antiprism (D_{4d})	2.223	2.583	2.122
	Triangular dodecahedron (D_{2d})	0.742	0.612	0.750
	Johnson gyrobifastigium J26 (D_{2d})	14.364	14.400	14.445
	Johnson elongated triangular bipyramid J14 (D_{3h})	29.261	30.258	29.087
	Biaugmented trigonal prism J50 (C_{2v})	2.916	3.170	3.082
	Biaugmented trigonal prism (C_{2v})	2.103	2.563	2.236
	Snub diphenoid J84 (D_{2d})	3.175	3.147	3.301
	Triakis tetrahedron (T_d)	11.089	10.870	10.769
	Elongated trigonal bipyramid (D_{3h})	23.607	23.653	22.892

Table S8. The CShM values calculated by SHAPE 2.1 for **Dy_2**.

Central atom	Coordination Geometry	**Dy1**
Dy	Octagon (D_{8h})	28.114
	Heptagonal pyramid (C_{7v})	24.789
	Hexagonal bipyramid (D_{6h})	13.943
	Cube (O_h)	12.505
	Square antiprism (D_{4d})	3.675
	Triangular dodecahedron (D_{2d})	2.855
	Johnson gyrobifastigium J26 (D_{2d})	8.982
	Johnson elongated triangular bipyramid J14 (D_{3h})	26.918
	Biaugmented trigonal prism J50 (C_{2v})	2.610
	Biaugmented trigonal prism (C_{2v})	1.721
	Snub diphenoid J84 (D_{2d})	2.908
	Triakis tetrahedron (T_d)	13.208
	Elongated trigonal bipyramid (D_{3h})	22.449

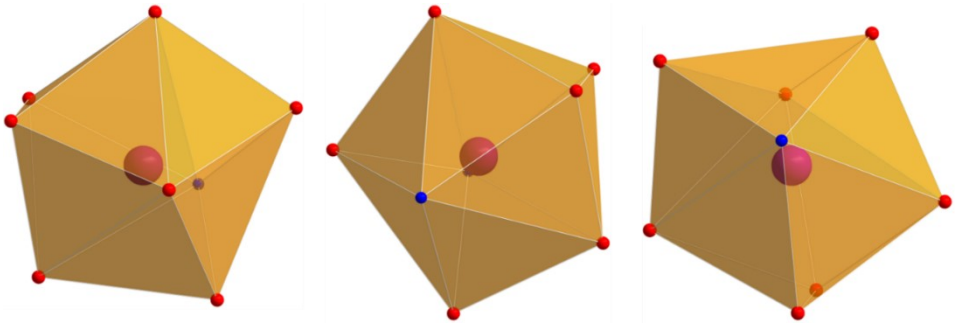

Figure S8. Coordination polyhedrons of Dy^{III} ions in complex **Dy_3**. The purple, red, and blue spheres represent Dy, O, and N, respectively.

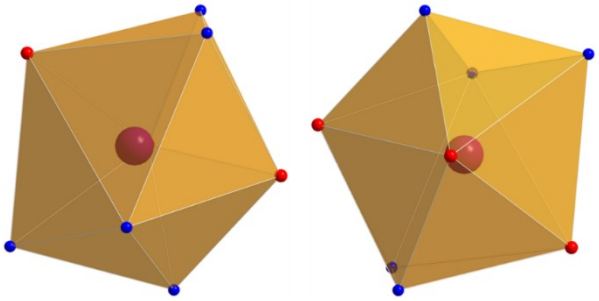

Figure S9. Coordination polyhedrons of Dy^{III} ions in complex **Dy_2**. The purple, red, and blue spheres represent Dy, O, and N, respectively.

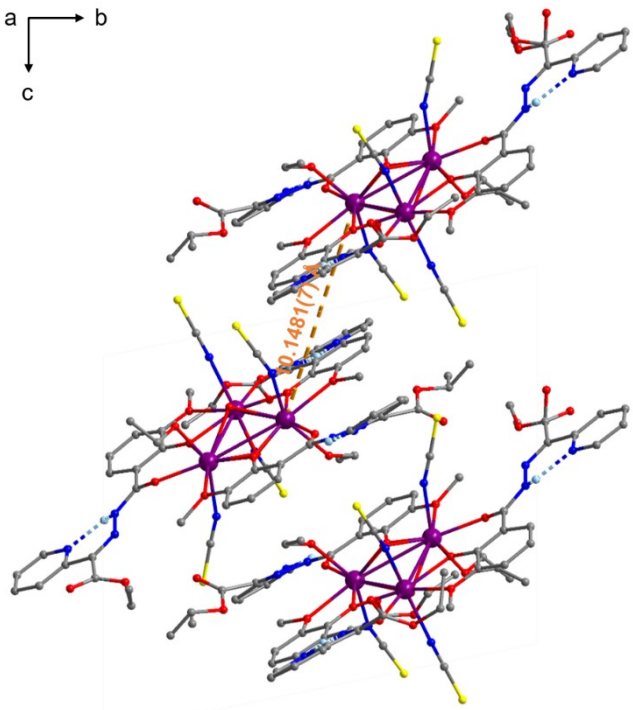

Figure S10. The packing diagram for **Dy_3** shown along the crystallographic *a* axis gives the shortest intermolecular Dy···Dy distance of 10.1481(7) Å. The purple, blue, light blue, red, yellow and gray spheres represent Dy, N, H, O, S and C, respectively; hydrogen atoms except for those involved in hydrogen bonding have been omitted for clarity.

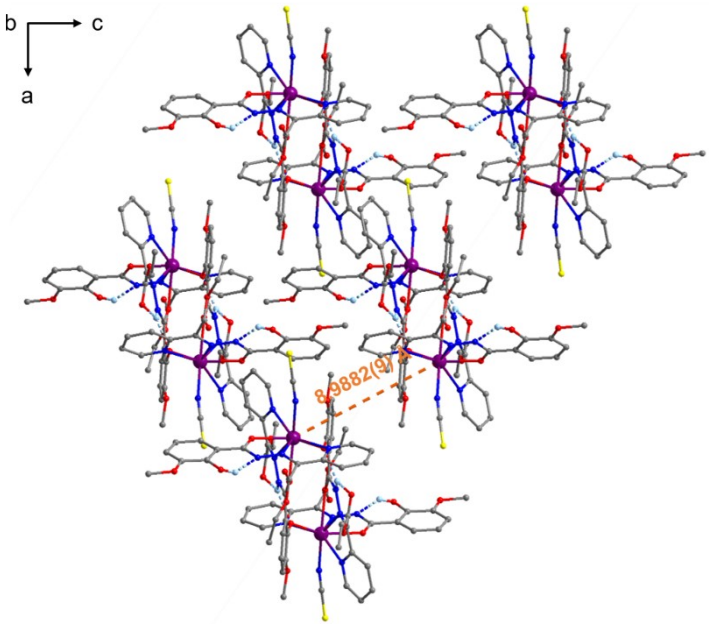

Figure S11. The packing diagram for **Dy_2** shown along the crystallographic *b* axis gives the shortest intermolecular Dy···Dy distance of 8.9882(9) Å. The purple, blue, light blue, red, yellow and gray spheres represent Dy, N, H, O, S and C, respectively; hydrogen atoms except for those involved in hydrogen bonding have been omitted for clarity.

3. Magnetic measurements

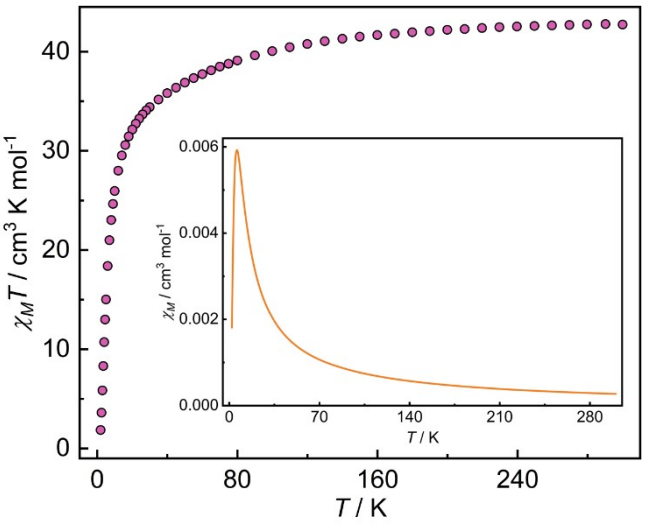

Figure S12. Plot of $\chi_M T$ versus temperature for **Dy_3** in an applied magnetic field of 1 kOe.

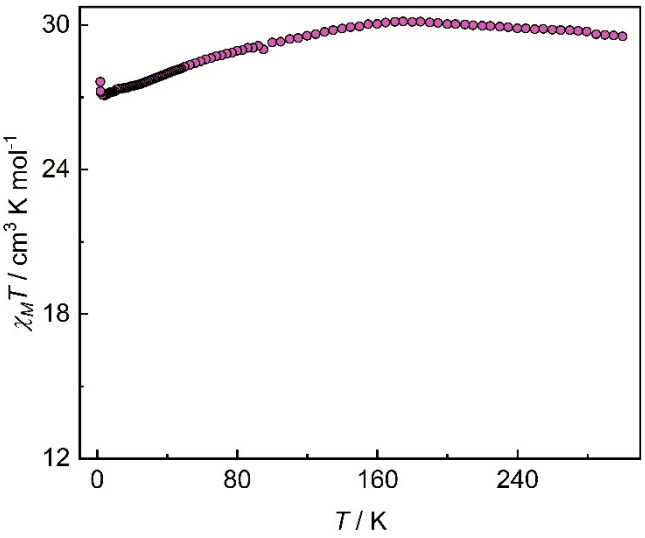

Figure S13. Plot of $\chi_M T$ versus temperature for **Dy_2** in an applied magnetic field of 1 kOe.

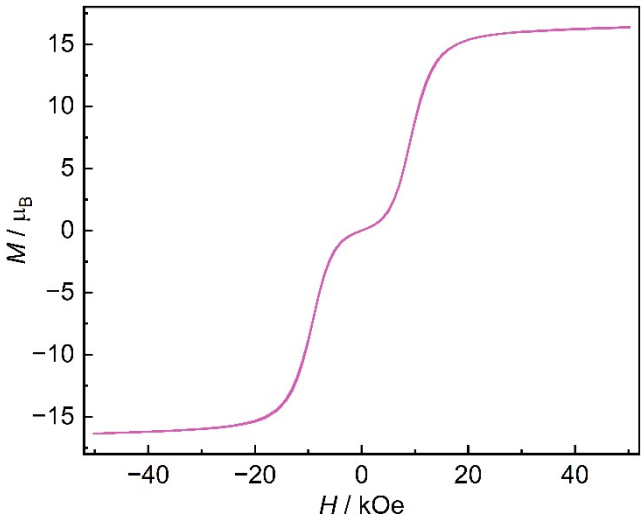

Figure S14. *M*(*H*) hysteresis loops for **Dy_3** in the temperature of 1.9 K using a sweep rate of 44 Oe/s.

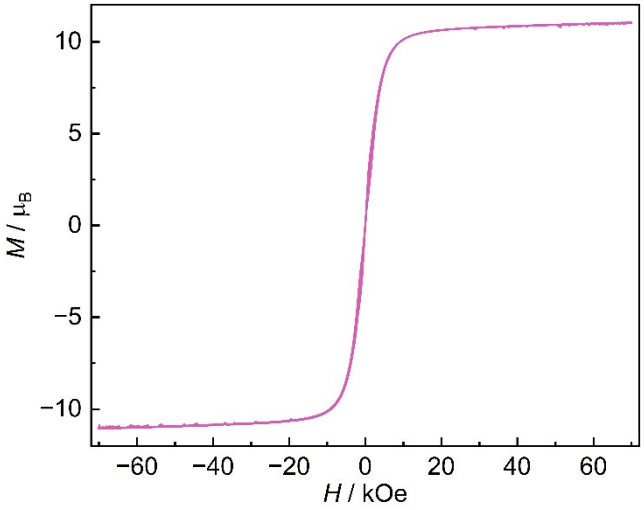

Figure S15. *M*(*H*) hysteresis loops for **Dy_2** in the temperature of 1.9 K using a sweep rate of 44 Oe/s.

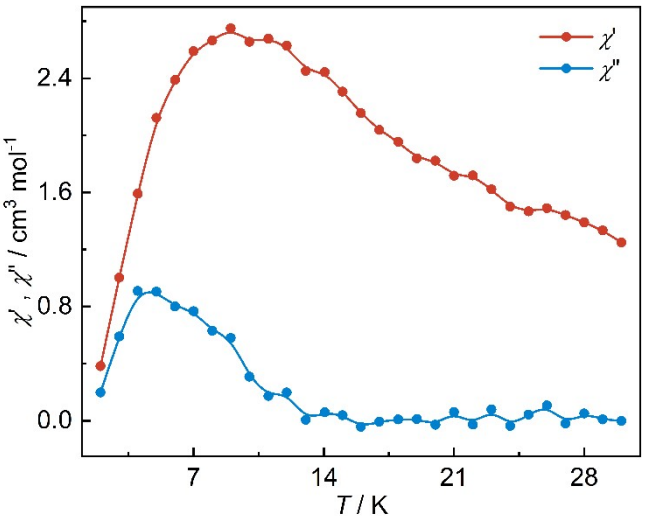

Figure S16. Temperature dependence of in-phase (χ') and out-of-phase (χ'') susceptibility for **Dy_3** in zero dc field.

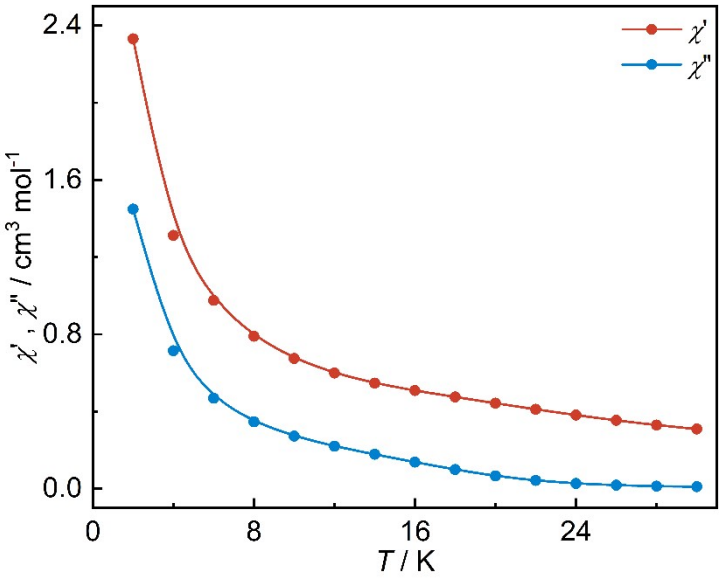

Figure S17. Temperature dependence of in-phase (χ') and out-of-phase (χ'') susceptibility for **Dy_2** in zero dc field.

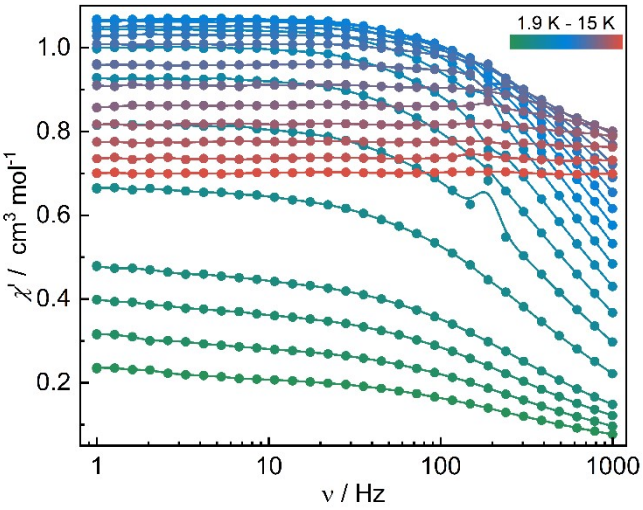

Figure S18. Frequency dependence of in-phase (χ') susceptibility for **Dy_3** in zero dc field.

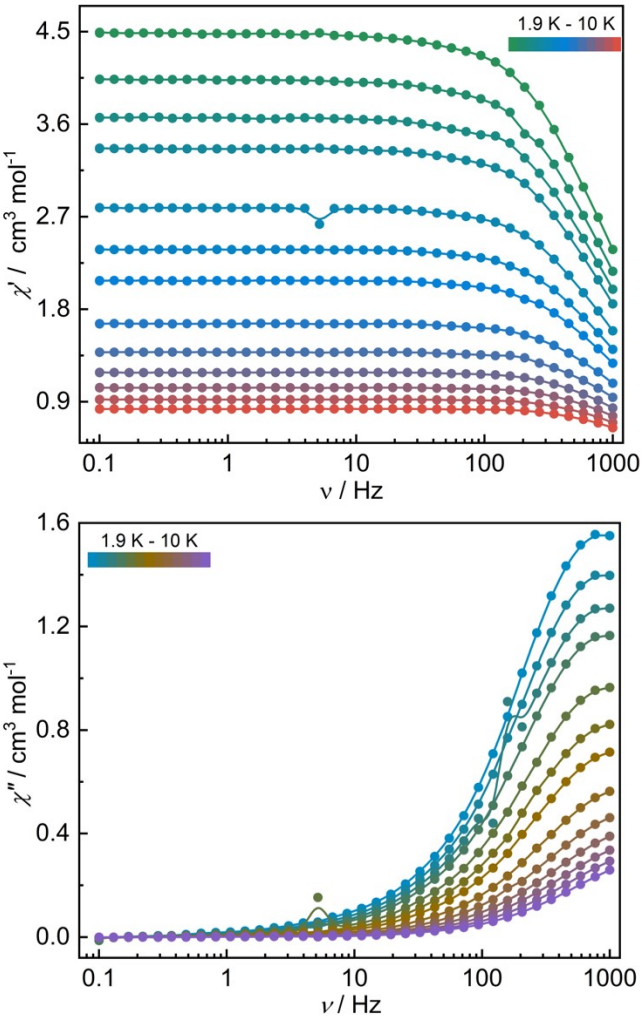

Figure S19. Frequency dependence of in-phase (χ') (up) and out-of-phase (χ'') (bottom) susceptibility for **Dy_2** in zero dc field.

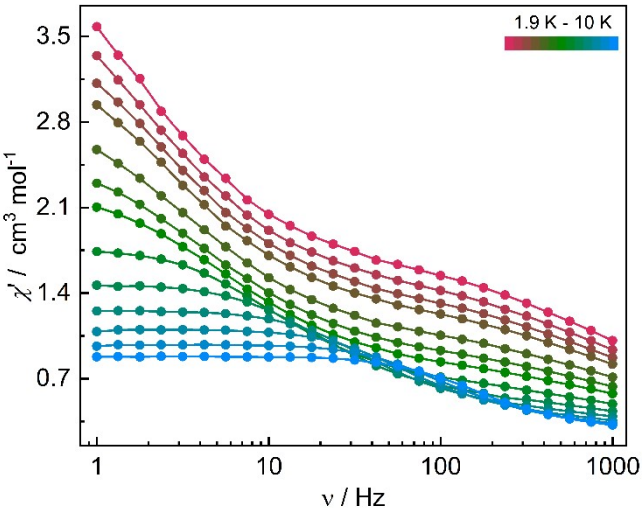

Figure S20. Frequency dependence of in-phase (χ') susceptibility for **Dy_2** in 400 Oe dc field.

Table S9. The relaxation fitting parameters for $\mathbf{Dy_3}$ from fitting ac data at varying temperatures.

T (K)	χ_S	χ_T	τ	α
1.9	0.162811E-13	0.245705E+00	0.571410E-03	0.512863E+00
2.1	0.198018E-13	0.318852E+00	0.525604E-03	0.451662E+00
2.3	0.245705E-13	0.399535E+00	0.490505E-03	0.413347E+00
2.5	0.304622E-13	0.480456E+00	0.455887E-03	0.387262E+00
3.0	0.350195E-13	0.674702E+00	0.377335E-03	0.342282E+00
3.5	0.462936E-13	0.830413E+00	0.305126E-03	0.313226E+00
4.0	0.601105E-13	0.944007E+00	0.267626E-03	0.307071E+00
4.5	0.816532E-13	0.101853E+01	0.230053E-03	0.305246E+00
5.0	0.131414E-12	0.106104E+01	0.196240E-03	0.291668E+00
5.5	0.177057E-12	0.108200E+01	0.166698E-03	0.297863E+00
6.0	0.236745E-12	0.108431E+01	0.140344E-03	0.294439E+00
6.5	0.314025E-12	0.107833E+01	0.117199E-03	0.296831E+00
7.0	0.490085E-12	0.106289E+01	0.951107E-04	0.303786E+00
7.5	0.835721E-12	0.104208E+01	0.765962E-04	0.297359E+00
8.0	0.127813E-11	0.101911E+01	0.608988E-04	0.294801E+00
9.0	0.208684E-11	0.966505E+00	0.367649E-04	0.293140E+00
10.0	0.362274E-11	0.915016E+00	0.228667E-04	0.264340E+00
11.0	0.597965E-11	0.864752E+00	0.146570E-04	0.217214E+00
12.0	0.103690E-10	0.818706E+00	0.881911E-05	0.192143E+00
13.0	0.154061E-10	0.776158E+00	0.541124E-05	0.174426E+00
14.0	0.485195E-10	0.736837E+00	0.420049E-05	0.121169E+00
15.0	0.677862E-10	0.701509E+00	0.300699E-05	0.966544E-01

Table S10. The relaxation fitting parameters for $\mathbf{Dy_2}$ from fitting ac data at varying temperatures in 400 Oe dc field.

T (K)	χ_S	χ_T	τ	α
1.9	1.49687	4.9642	0.09799	0.30601
2.1	1.37321	4.33035	0.08371	0.32245
2.3	1.25695	3.98368	0.07139	0.32806
2.5	1.16972	3.659	0.0627	0.32395
3.0	0.95187	3.08929	0.04615	0.32542
3.5	0.84083	2.64078	0.03472	0.31867
4.0	0.74974	2.30097	0.02554	0.25531
5.0	0.691	1.78003	0.01345	0.21009
6.0	0.55345	1.47567	0.00696	0.15264
7.0	0.4791	1.25836	0.00386	0.14321
8.0	0.34621	1.10664	0.00226	0.13518
9.0	0.30605	0.98114	0.0014	0.08282
10.0	0.284361	0.885591	9.44018E-4	0.06581

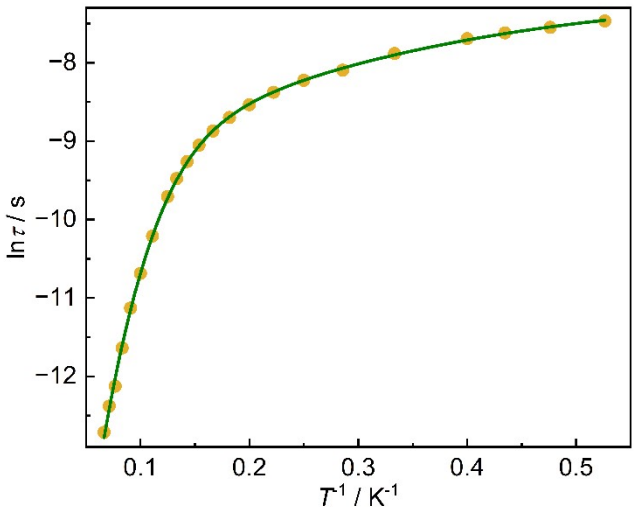

Figure S21. Temperature dependence of the relaxation time in the form of natural logarithm for **Dy_3**. The green line represents the fit. The fitting equation is $\ln(\tau) = -\ln[CT^n + \tau_0^{-1}\exp(-U_{eff}/k_BT) + \tau_{QTM}^{-1}]$.

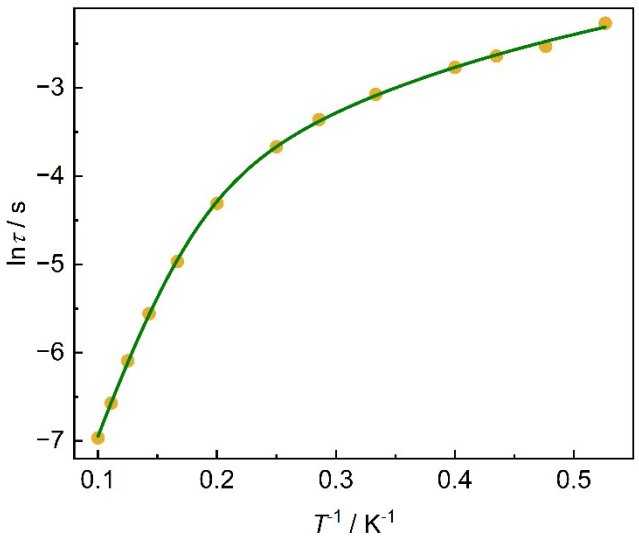

Figure S22. Temperature dependence of the relaxation time in the form of natural logarithm for **Dy_2** in 400 Oe dc field. The green line represents the fit. The fitting equation is $\ln(\tau) = -\ln[AT + CT^n + \tau_0^{-1}\exp(-U_{eff}/k_BT)]$.

4. References

[1] Y.-N. Guo, G.-F. Xu, P. Gamez, et al., Two-Step Relaxation in a Linear Tetranuclear Dysprosium(III) Aggregate Showing Single-Molecule Magnet Behavior, J. Am. Chem. Soc., 2010, 132, 8538-8539.

[2] S. Roy, S. K. Das B. Chattopadhyay, Cobalt(II)-based Metalloradical Activation of 2-(Diazomethyl)pyridines for Radical Transannulation and Cyclopropanation, Angew. Chem. Int. Ed., 2018, 57, 2238-2243.

[3] E. A. Boudreaux L. N. Mulay, Theory and applications of molecular paramagnetism John Wiley & Sons, New York, 1976.

[4] O. V. Dolomanov, L. J. Bourhis, R. J. Gildea, et al., OLEX2: a complete structure solution, refinement and analysis program, J. Appl. Crystallogr., 2009, 42, 339-341.

[5] G. Sheldrick, Crystal structure refinement with SHELXL, Acta Crystallogr. Sect. C, 2015, 71, 3-8.

[6] G. Sheldrick, SHELXT - Integrated space-group and crystal-structure determination, Acta Crystallogr. Sect. A, 2015, 71, 3-8.

[7] M. Pinsky D. Avnir, Continuous Symmetry Measures. 5. The Classical Polyhedra, Inorg. Chem., 1998, 37, 5575-5582.

[8] D. Casanova, J. Cirera, M. Llunell, et al., Minimal Distortion Pathways in Polyhedral Rearrangements, J. Am. Chem. Soc., 2004, 126, 1755-1763.